Transport in Porous Media (2020) 134:331–349
https://doi.org/10.1007/s11242-020-01448-3

Oil Reservoir on a Chip: Pore-Scale Study of Multiphase Flow During Near-Miscible CO_2 EOR and Storage

Mojtaba Seyyedi[1] · **Mehran Sohrabi**[2]

Received: 8 September 2019 / Accepted: 7 July 2020 / Published online: 21 July 2020

Abstract

CO_2 injection into oil reservoirs is widely accepted as an effective enhanced oil recovery and CO_2 storage technique. While oil recovery and CO_2 storage potential of this technique have been studied extensively at the core-scale, complex multiphase flow and fluid–fluid interactions at the pore scale during near-miscible CO_2 injection have not, and this area needs more study. To address this, a unique high-pressure microfluidic system was implemented which allows for the optical visualisation of the flow using optical microscopy. The results show that during tertiary near-miscible CO_2 injection, when CO_2 phase contacts the oil, the oil spreads as a layer between the CO_2 phase and water preventing CO_2 phase from contacting the water phase. This is attributed to the positive value of the spreading coefficient. Furthermore, due to the presence of pore-scale heterogeneity in the chip, an early breakthrough of CO_2 was observed causing a large amount of oil to be bypassed. However, after CO_2 breakthrough, CO_2 gradually started to diffuse and flow inside the bypassed oil zones in the transverse directions which is a characteristic of capillary crossflow. The driving force for this capillary crossflow was the interfacial tension gradient formed by the diffusion of CO_2 into the oil phase and the extraction of light to medium hydrocarbon components from the oil into the CO_2 phase. The same mechanism led to the recovery of the bypassed oil trapped in dead-end pores. This unique mechanism produced the majority of the bypassed oil after CO_2 breakthrough and significantly increased the oil recovery. In our three-phase flow water-wet system, CO_2 flow displaced the water through a multiple displacement mechanism which is unique to three-phase flow. CO_2 displaced the oil in oil-filled pores thorough bulk flow, and the spreading oil layers were gradually produced by layer flow.

Keywords Near-miscible · Miscibility · Capillary crossflow · Spreading coefficient · Layer flow

✉ Mojtaba Seyyedi
Mojtaba.seyyedi@csiro.au

[1] CSIRO Energy, Australian Resources Research Centre (ARRC), 26 Dick Perry Avenue, Kensington, WA 6151, Australia

[2] Centre for Enhanced Oil Recovery and CO2 Solutions, Heriot-Watt University, Edinburgh, UK

1 Introduction

With the continuous increase in atmospheric CO_2 concentration, interest in underground CO_2 storage has been raised. While there is a motivation to store CO_2 in underground formations, there is a need to enhance the oil recovery from the majority of mature oil fields. Primary oil recovery in the majority of oil reservoirs is low. Even after waterflooding, a significant amount of oil will remain in place. The average global oil recovery factor by waterflooding is in the range of 45–50% of the original oil in place (Sandrea and Sandrea 2007). One promising scenario to produce some part of the residual oil is through CO_2 injection. CO_2 injection is the most well-known enhanced oil recovery (EOR) scenario and has been applied in various oil fields around the world. In the USA, the Permian Basin has been under CO_2 injection for around 50 years (Tenasaka 2011). By injecting CO_2 into the oil reservoirs, some volume of the injected CO_2 will be trapped and retained in the reservoir due to its dissolution into the formation brine (Mojtaba et al. 2014) and crude oil, geochemical reactions (Welch et al. 2018; Seyyedi et al. 2020a, b) and capillary and structural trapping (Seyyedi et al. 2020b; Al-Menhali and Krevor 2016). Therefore, by injecting CO_2 into oil reservoirs not only the CO_2 can be safely stored underground but additional oil can be produced that creates a revenue stream for the storage operation (Bachu 2003, Kuuskraa et al. 2013; Hill et al. 2013).

According to previous studies (Nobakht et al. 2008; Yongmao et al. 2004), CO_2 injection into oil reservoirs can enhance the oil recovery through three major oil recovery mechanisms which are oil swelling, oil viscosity reduction and development of miscibility. Miscibility occurs only if the reservoir pressure is above the minimum miscibility pressure (MMP) for the crude oil and CO_2 at a given reservoir temperature. Under the miscible condition, the maximum oil recovery by CO_2 injection can be obtained (Metcalfe and Yarborough 1979). However, not all the oil reservoirs have pressures above MMP. Some of them have pressures much lower than MMP, and some have pressures slightly lower than MMP (near-miscible condition), and therefore, their crude oils are immiscible with CO_2 under reservoir conditions. Moreover, the presence of impurities such as N_2 and methane will negatively impact the MMP value (Zhang et al. 2004; Metcalfe 1982). The presence of these impurities in CO_2 stream is common as making a purified CO_2 stream is expensive (Zhang et al. 2004). Therefore, although a reservoir may have a pressure above MMP when purified CO_2 is used, it may have a near-miscible condition when the CO_2 stream has impurities. Several researchers (Grigg et al. 1997; Shyeh-Yung 1991) have shown that when the reservoir pressure is below the MMP, the CO_2 oil recovery potential decreases as a result of the loss of miscibility. Under this condition, CO_2 injection as an EOR scenario may not be considered viable for these reservoirs as a low pore-scale displacement, and thus, low oil recovery is expected. As such, little attention has been given to near-miscible CO_2 flooding and its oil recovery mechanisms.

Furthermore, so far, oil recovery potential of CO_2 injection under different injection scenarios (i.e. huff and puff, continuous CO_2 injection or CO_2–water alternating gas (WAG) injection) has been mainly investigated through core flooding studies (Huang et al. 2017; Ghasemi et al. 2018; Seyyedsar and Sohrabi 2017; Zhang et al. 2018; Ma et al. 2016). Core flooding is a powerful tool for evaluating the oil recovery potential of almost any EOR scenario; however, due to its "black box" nature, little information regarding the multiphase flow behaviour, displacement mechanisms and fluid–fluid interactions at pore scale can be obtained. Medical X-ray CT can be used to capture more data from the experiments (Tovar et al. 2014; Akai et al. 2015; Khather et al. 2018). Unfortunately, the voxel size of the medical CT rigs is

usually around $0.13 * 0.13 * 0.4$ mm^3 which is not sufficient to reveal the fluids flow behaviour, displacement mechanisms and fluid–fluid interactions taking place at the pore scale. Micro-CT rigs for coreflooding tests have better resolution (Rahman et al. 2016; Perrin and Benson 2010; Li et al. 2015) with the majority of studies focused on either brine–CO_2 interaction or CO_2 capillary trapping (Rahman et al. 2016; Perrin and Benson 2010; Li et al. 2015). Furthermore, flooding experiments conducted in micro-CT are very time-consuming and expensive.

In this study, a microfluidic approach is used to investigate CO_2–oil interactions, oil recovery and displacement mechanisms at pore scale under reservoir pressure and temperature. Using this tool, we have directly observed the phenomena that take place at the pore scale during and after injection. Using this approach, Sohrabi et al. (2009), Seyyedi et al. (2017a, 2019) and Seyyedi and Sohrabi (2017) investigated the oil recovery mechanisms and fluids flow in porous media during carbonated (CO_2-saturated) brine injection at various reservoir conditions. AlQuaimi and Rossen (2018) studied foam flow in a porous medium. Song ad Kovscek (2015) used a kaolinite functionalized chip to study the oil recovery process of low salinity brine injection.

Robin et al. (2012) studied fluid distribution during immiscible CO_2 injection into a microfluidic chip under different wettability conditions. Their study was mainly focused on the role of the spreading coefficient on CO_2 oil recovery. In their observation, they observed oil spreading on the brine and asphaltene precipitation as a result of CO_2–oil interactions. Work published by Hamidi and Awang (2017) focused on oil recovery by low-temperature CO_2 injection into a high-temperature reservoir using a microfluidic chip. Their results showed that this injection method can increase the oil recovery which is attributed to the CO_2 expansion in the porous medium that leads to stronger invasion of oil-filled pores by CO_2. Sohrabi et al. (2008) investigated the oil recovery mechanisms of secondary and tertiary near-miscible methane injection in a microfluidic chip partially saturated with n-decane. Their results showed significant oil recovery potential for near-miscible methane injection with better performance for the secondary scenario compared to tertiary recovery. They reported a strong crossflow of bypassed oil into the main flow stream leading to good recovery of the CH_4-contacted decane. As they used methane and a model oil (i.e. *n*-decane), their results cannot be necessarily applied to the case of CO_2 injection in a live reservoir crude oil system where multiple-contact miscibility is the typical mechanism by which miscibility is reached. Seyyedi et al. (2017b) through a series of phase behaviour (i.e. PVT) and microfluidic experiments investigated the oil compositional variations that occur during carbonated brine and CO_2 injection EOR scenarios. Their results showed that the strong extraction of oil components that happen during CO_2 injection does not occur with carbonated brine injection.

As shown above, little information exists regarding the multiphase flow, fluid displacement mechanisms and fluid–fluid interactions at the pore scale during near-miscible CO_2 EOR/storage in oil reservoirs. This study aims to address these shortcomings in the scientific literature. An in-house designed high-pressure and high-temperature microfluidic rig was used. The experiments were performed under the pressure of 2500 psi and temperature of 37.8 °C (achieving supercritical CO_2) using a live reservoir crude oil.

Table 1 Properties of used crude oil

Saturates (wt%)	Aromatics (wt%)	Resins (wt%)	Asphaltenes (wt%)
30.00	40.10	24.20	5.70

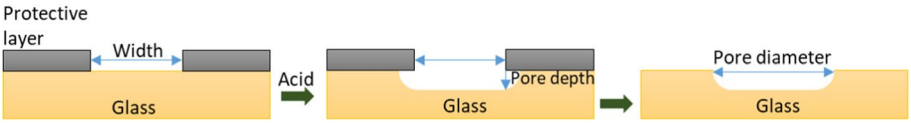

Fig. 1 Schematic of wet etching method with hydrogen fluoride

2 Materials and Methods

2.1 Materials

As the majority of oil fields have live crude oil (oil with dissolved gas) (Ahmed 2013), a live crude oil was utilized in this work. The dissolved gas in most live crude oils is mainly methane (Ahmed 2013). Therefore, to make the live crude oil, a reservoir crude oil with an API of 22 was fully saturated with methane at a pressure of 2450 psi and a temperature of 37.8 °C using a rocking cell. The saturation pressure was chosen 50 psi lower than test pressure to avoid any gas nucleation due to possible slight pressure variations. The methane content of live crude oil was around 30 mol%. The MMP of this live crude oil with pure CO_2 was estimated to be around 2800 psi. The oil properties are shown in Table 1. The CO_2 solubility in this oil at test conditions is 54 mol%. The live (CH_4-saturated) oil viscosity at test conditions was around 12 cP.

A brine with a total salinity of 10,000 ppm (8000 ppm NaCl and 2000 ppm $CaCl_2$) was used for the waterflooding step. As the oil was fully saturated with methane, to avoid any methane mass transfer between the oil and brine, the brine was fully saturated with methane at the pressure of 2450 psi and temperature of 37.8 °C. The methane content of live brine was around 0.2 mol%. CO_2 with a purity of 99.99 mol% was used in this work. The CO_2 viscosity at test conditions was around 0.07 cP. The CO_2 solubility in used brine at test conditions was around 2 mol%.

3 Method

3.1 Glass Chip Fabrication

A random porous pattern was fabricated on a glass with a very smooth surface using a wet etching method with hydrogen fluoride (Ceyssens and Puers 2009) (Fig. 1). This porous pattern was used on purpose since it has permeability heterogeneities which mimic low sweep efficiency for waterflooding causing oil to be bypassed. This replicates the low performance of waterflooding in oil reservoirs. The average pore depth of the etched substrate measured by a light scattering method was estimated at 50 μm and the pore–throat

Table 2 Microfluidic chip properties

Length (cm)	Width (cm)	Pore volume (cm^3)	Porosity	Permeability (D)	Average pore depth (μm)	Pore diameter range (μm)
7	0.7	0.01	0.51	7	50	30–500

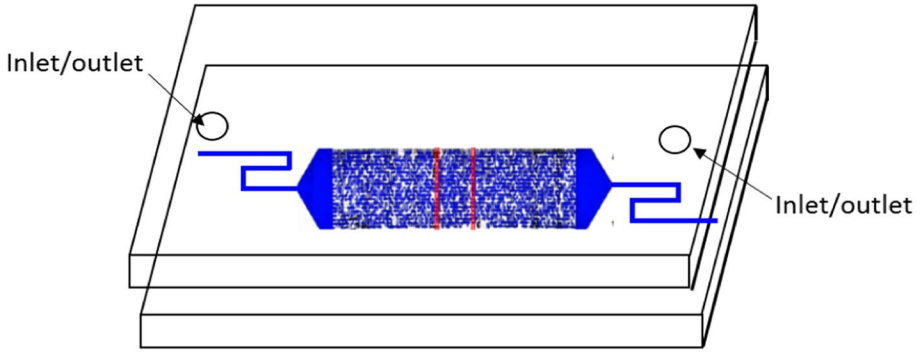

Fig. 2 Microfluidic chip

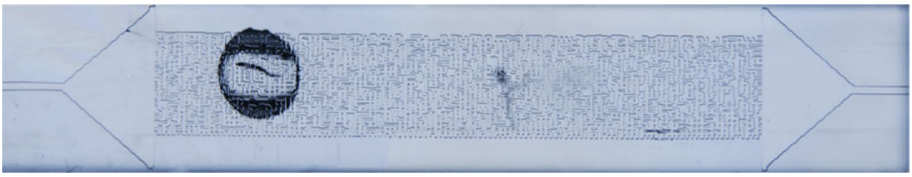

Fig. 3 The microfluidic chip before pressurizing the overburden fluid to remove the air bubbles

diameters ranged from 30 to 500 μm. The microfluidic chip dimensions are shown in Table 2.

A flat glass plate with a very smooth surface matching the size of the etched substrate was used to seal the system. After etching the glass, both etched and flat substrates were cleaned with detergent (Decon 90) and sonicated in deionized water for 15 min. The water was changed every 5 min. Next, the clean substrates were dried, and then, they were brought into contact (Fig. 2). As the glass substrates had outstanding flatness and very optically smooth surfaces, when they were combined, they attached strongly to each other. Next, the inlet and outlet ports were connected to the combined substrates (microfluidic chip) and the chip (Fig. 3) was placed inside a high-pressure visual chamber. The chamber was filled with glycerol oil. The pressure of glycerol oil was slowly increased to 400 psi using a high-resolution pump (Quizix Q5000 Series), while the pore pressure inside the microfluidic chip was kept at atmospheric conditions. The confining pressure on the microfluidic chip was kept constant for a few hours, while the pump flow rate was monitored. This step was done to ensure that the combined substrates do not leak and are completely sealed.

3.2 Microfluidic Rig

The schematic of the microfluidic rig is shown in Fig. 4. Initially, the pore pressure of the microfluidic chip was slowly increased by injecting deionized water into the chip while increasing the overburden pressure. A net confining pressure of 400 psi was always kept on the chip during the operation. The pore pressure of the chip was increased to 2500 psi which is the test pressure. The whole set-up was housed inside an oven with a visual

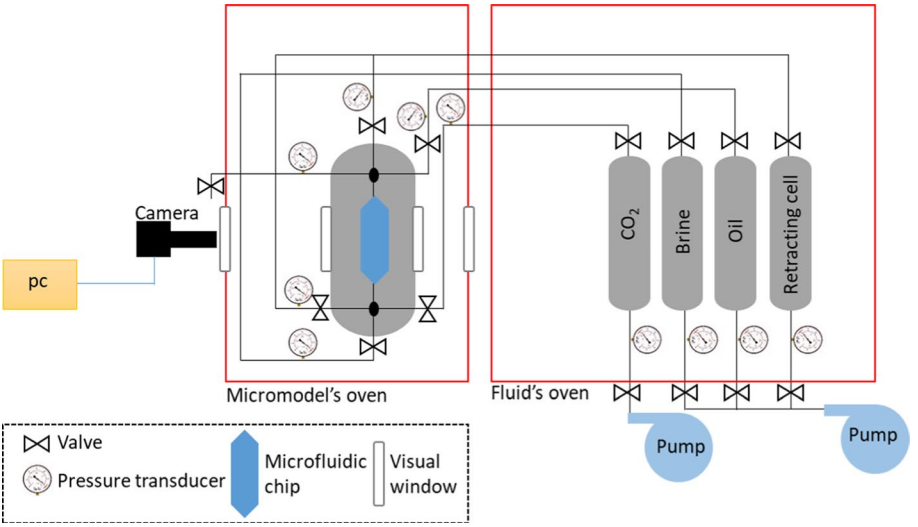

Fig. 4 Schematic of the high-pressure and high-temperature microfluidic rig

window. A separate oven at the same temperature was used for the fluids to minimize temperature variations during the experiment. Both ovens were kept at a temperature of 37.8 °C. Fluids were kept in high-pressure/temperature accumulators placed inside the corresponding oven. To keep the pressure of the accumulators at the test pressure and inject the fluids at low rates into the microfluidic chip, a series of high-resolution pumps (Quizix Q5000 Series) were used. To maintain the backpressure on the chip's pore pressure constant, the outlet of the chip was connected to a retraction cell that was connected to a pump (Quizix Q5000 Series) set on a constant pressure receive mode. A high-resolution microscope kit was utilized for capturing high-quality images and videos at the microscale during experiments. The microscope had a built-in fine focus. The kit was fixed at the desired position by utilizing a manual camera mount and positioning system. The camera was connected to a PC where Streampix software was used for recording videos and pictures.

3.3 Experimental Procedure

Since any type of pore patterns can be etched onto the glass and any live fluids can be used in this rig, multiphase flow behaviour, displacement mechanisms and fluids phase behaviour occurring in the oil reservoirs can be well identified by using this microfluidic rig. Prior to the test, the micromodel chip was thoroughly cleaned by acetone, toluene and methanol. Next, it was dried by N_2 and vacuumed. Then, it was fully saturated with brine at test conditions and brine was displaced by CH_4-saturated brine. Then, live crude oil was injected from the bottom of the chip towards its top to establish the initial water and oil saturation. This step replicates oil migration into a sedimentary formation and displacement of the brine with oil that created the oil reservoir itself.

To replicate waterflooding operations in oil fields, CH_4-saturated water was injected into the chip from the bottom port, while fluids (oil and brine) were produced from the top port. Usually, in field applications, waterflooding continues until the water-cut passes a specific value and oil production is no longer economically viable. In the laboratory, we do not

have such limitations and the waterflooding stage was continued until oil recovery completely ceased. As mentioned in the introduction section, to produce the trapped oil in an oil reservoir after the waterflooding step (i.e. secondary flooding), an enhanced oil recovery scenario such as CO_2 injection will be applied. To mimic this case, CO_2 was injected from the bottom port of the model and the fluids (brine, oil and CO_2) were produced from the top port. The injection was continued until oil recovery was ceased. During the whole operation, images and videos from the fluids inside the chip were frequently recorded.

4 Results and Discussion

4.1 Waterflooding

As expected waterflooding of the chip led to very low oil recovery, and Fig. 5 shows a significant amount of oil was bypassed by water and remained in the porous medium after oil production had completely ceased. Figure 6 is a close-up image showing that the chip wettability state was mainly water-wet. Having analysed the captured images and videos, there are some areas in the chip showing indications of neutral wetting conditions; however, the majority of the chip shows a water-wet behaviour.

4.2 Tertiary Near-Miscible CO_2 Injection

Interestingly, during tertiary near-miscible CO_2 injection, oil spread between water and CO_2 interfaces preventing contact between the CO_2 phase and water. This behaviour shown in Figs. 7 and 8 can be attributed to the positive value of the spreading coefficient (SC). The spreading coefficient can be measured as:

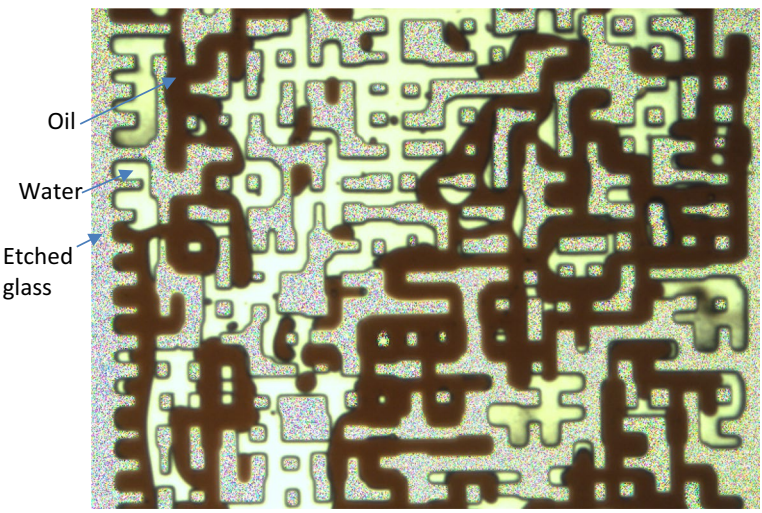

Fig. 5 Significant amounts of oil remained in the porous medium after waterflooding had been completed (i.e. oil production had ceased)

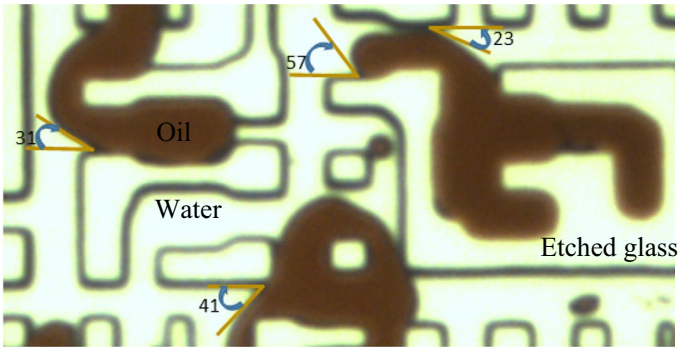

Fig. 6 Close-up view of the chip at the end of water flooding showing the wettability state was mainly water-wet

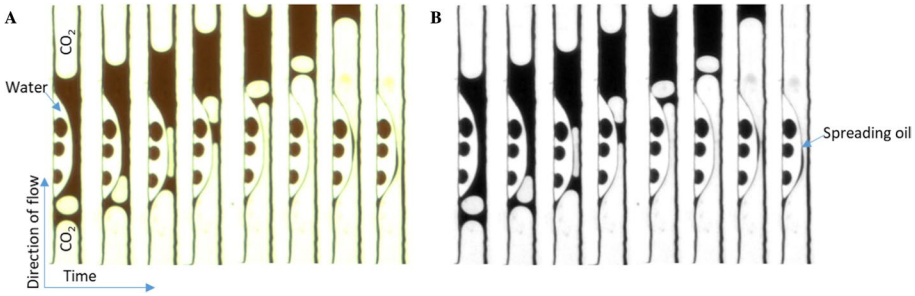

Fig. 7 CO_2 flow in a pore with trapped water-shielded oil ganglia. CO_2 phase flows inside the oil, and the oil phase spreads between the CO_2 phase and water. To better indicate the presence of oil layer between the CO_2 phase and water, figure (**a**) was turned to black and white (**b**)

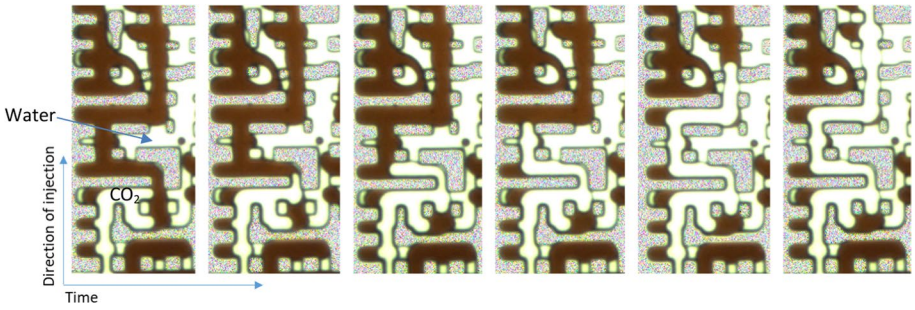

Fig. 8 Images showing oil spreading over CO_2 preventing the contact of the CO_2 phase with water

$$SC = \gamma_{CO_2\text{-water}} - \gamma_{CO_2\text{-oil}} - \gamma_{\text{oil-water}} \quad (1)$$

where γ is the interfacial tension (IFT) between the phases (CO_2, water and oil). For immiscible and near-miscible gas injection scenarios, depending on the spreading coefficient value and the wettability state of the system, the gas phase can spread differently between the water and oil which directly affects the surface contact area of the gas phase

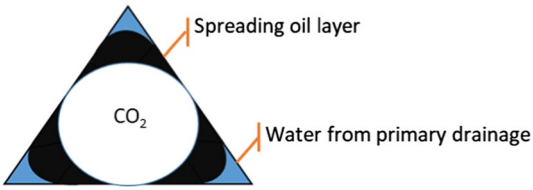

Fig. 9 Fluids configuration in a three-phase flow water-wet system with SC > 0

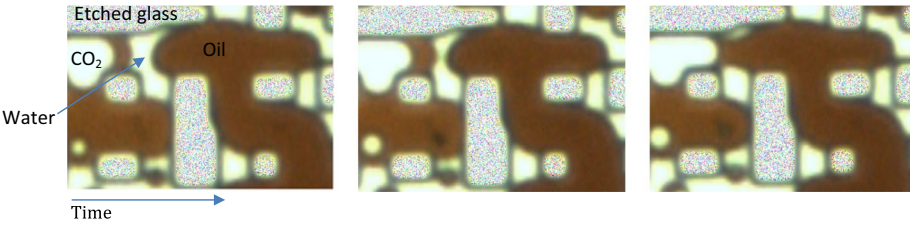

Fig. 10 Reconnection of isolated oil ganglia through double drainage mechanism

with the oil and therefore the oil recovery. Maximum oil recovery occurs when the oil has maximum contact with CO_2 phase (i.e. SC > 0, where the CO_2 phase is flowing inside the oil and the oil is spread on the CO_2 phase). In a water-wet porous medium when SC > 0, oil forms a layer between water occupying the corners and cervices and the gas phase flowing at the centre of the pore. This fluids' configuration is shown in Fig. 9. Therefore, the hydrocarbon phase, which is spread as a layer between water and gas interfaces, prevents direct contact between the CO_2 phase and water.

As shown in Eq. 1, one determining factor on the spreading coefficient value is the IFT between the oil and CO_2 ($\gamma_{CO2\text{-}oil}$). As it has been shown by several researchers (Nemati Lay et al. 2006; Hemmati-Sarapardeh et al. 2014; Golkari and Riazi 2017), as the pressure increases, the IFT between CO_2 and crude oil decreases, and at near-miscible conditions, very low IFTs between CO_2 and crude oil are expected as opposed to the immiscible condition where high IFTs between oil and CO_2 exist. The lower IFT between CO_2 and crude oil favours the spreading coefficient and therefore the oil recovery.

As shown in Fig. 5, the residual oil after waterflooding step is in the form of bypassed residual oil and/or disconnected oil ganglia surrounded by water. When CO_2 injection was started, it flowed in the porous medium inside the oil phase and was surrounded by oil layers, and oil was pushed ahead of the CO_2. Therefore, each pore was first filled with the oil (1st drainage), and then, CO_2 invaded the pore (2nd drainage). This is a double drainage event since the chip was water-wet. During this three-phase flow, CO_2 displaced the brine through a multiple displacement mechanism. Multiple displacements refer to several piston events, where a CO_2 segment displaces an oil segment which in turn displaces a brine segment as shown in Fig. 10. Because of this three-phase flow mechanism, some of the isolated oil ganglia were reconnected and an oil bank was formed ahead of the CO_2 front that led to further redistribution and reconnection of other isolated oil ganglia. This three-phase flow at the pore scale is shown in Fig. 10.

During the tertiary CO_2 injection, an early breakthrough of CO_2 was observed. Figure 11 shows fluids distributions in the whole microfluidic chip just after CO_2 breakthrough. There is only one CO_2 flow path that is almost continuous in the entire section of the chip, while a significant amount of oil was bypassed (residual oil saturation = 0.64).

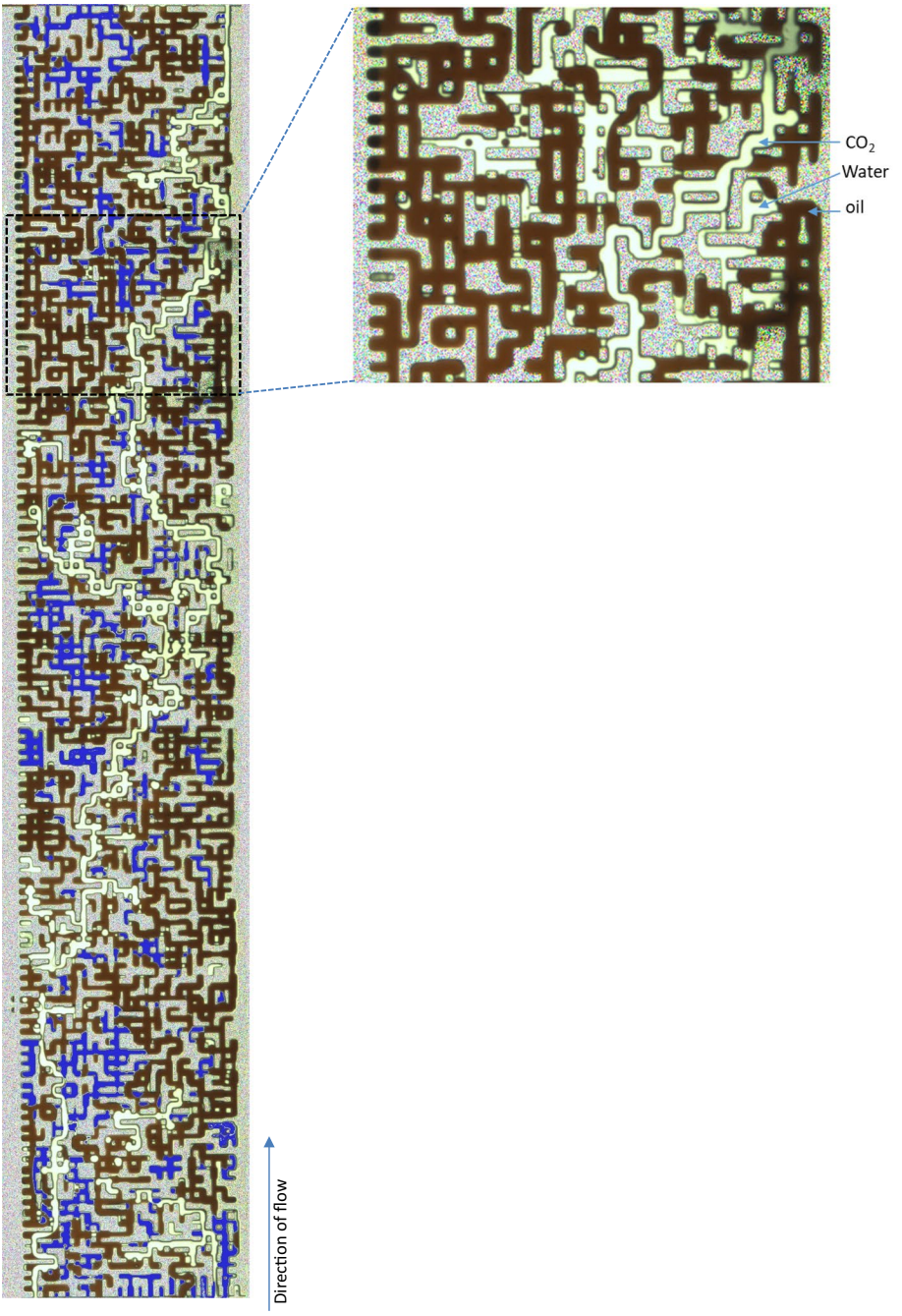

Fig. 11 Early breakthrough of CO_2 led to bypassing of a large volume of residual oil in the microfluidic chip. **a** To differentiate between water and CO_2, which both originally had a white colour, the water phase is digitally coloured in blue

This indicates that CO_2 flow was completely dominated by pore-scale heterogeneity of the chip. Due to the near-miscible condition of our system, although IFT between the oil and CO_2 is low, it is not zero. Therefore, there is a threshold entry pressure for each pore determined by the pore diameter. As such, CO_2 (the non-wetting phase) tends to flow through the easiest flow path determined by the entry pressures available at each stage of the advance of the CO_2. Once CO_2 establishes its easiest flow path (Fig. 11), it continues to flow through that path and diffuses to the bypassed oil contacted. Note that the adverse viscosity ratio (200 in our case) also plays a role in the early breakthrough of CO_2, but it is not the cause of the CO_2 flow path shown in Fig. 11.

As CO_2 diffuses into the bypassed oil contacted, initially the IFT between the CO_2 phase and oil decreases. However, soon after CO_2 breakthrough, CO_2 starts to extract the light-to-intermediate (extractable) oil components from the bypassed oil phase adjacent to the flowing CO_2 stream. This extraction leads to an IFT gradient across the oil phase with the highest IFT region which is placed at the CO_2–oil interface, and the lowest IFT is at the bulk of the oil phase away from the CO_2–oil interface. This IFT gradient leads to a capillary crossflow which causes the invasion of CO_2 into the bypassed oil and production of the oil through the spreading oil layer shown in Fig. 9. The same mechanism helps the production of the oil trapped in dead-end pores as shown in Fig. 12. This mechanism was also reported by Campbell and Orr (Campbell and Orr 1985) and is responsible for the significant extra oil recovery after CO_2 breakthrough as shown in Fig. 13. Around 50% of the undisplaced oil after CO_2 breakthrough was produced by the end of the test. During the CO_2 flow, CO_2 displaced the oil in oil-filled pores by bulk flow and the spreading oil layers were gradually produced by layer flow.

It should be noted that the IFT gradient across the oil phase decreases over time which is due to the depletion of the oil phase from its extractable oil components. As CO_2 phase extracts hydrocarbon components from the oil adjacent to the CO_2 phase, a concentration gradient of the extractable oil components in the oil phase will be formed which provides a driving force for the diffusion of extractable oil components through the oil phase towards the oil adjacent to the CO_2 phase and their consequent extraction to the CO_2 phase. When CO_2 has been flowing past undisplaced oil for an extended period, as the bulk of the oil phase gets depleted from the extractable oil components, the IFT gradient across the oil phase decreases. Therefore, the capillary crossflow becomes weaker and the rate of advancement of CO_2 meniscus into the bypassed oil zone decreases as shown in Fig. 12. Eventually, the oil will become depleted from the extractable oil components and IFT gradient across the undisplaced oil phase becomes zero and the capillary crossflow will be stopped, and the residual oil remains unproduced.

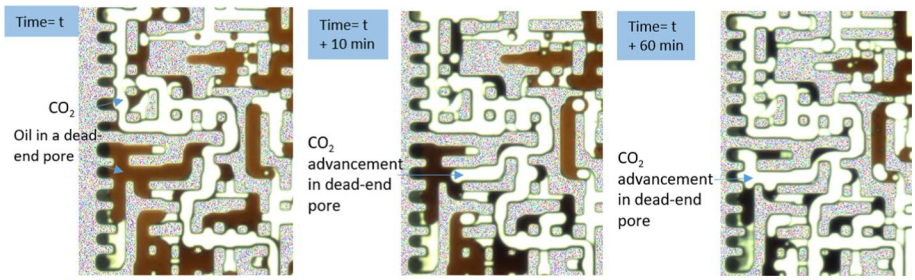

Fig. 12 Oil recovery by CO_2 capillary crossflow into the bypassed oil-filled pores

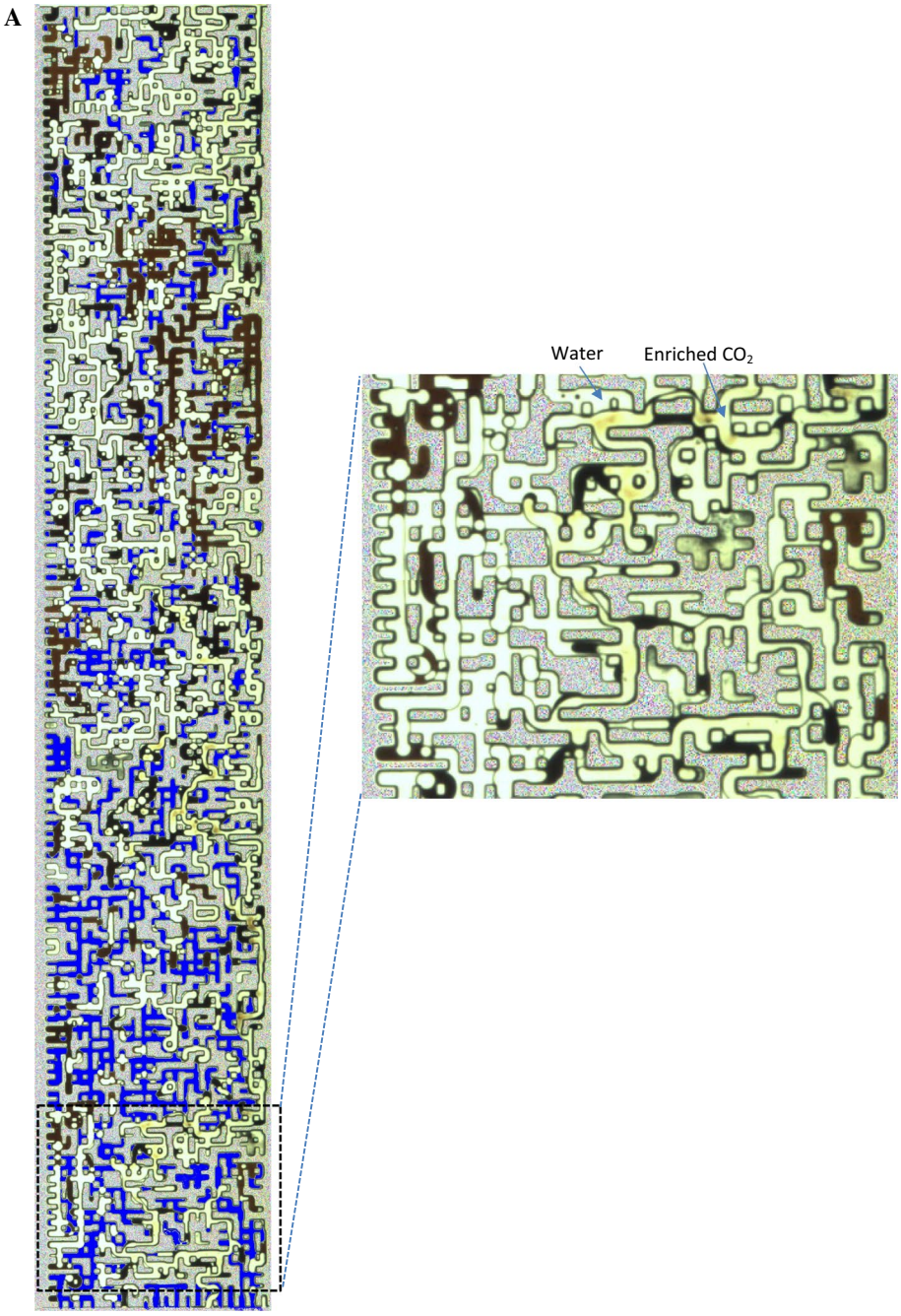

Fig. 13 Ultimate oil recovery after 24 h CO_2 injection. **a** To differentiate between water and CO_2, which both originally had a white colour, the water phase is digitally coloured in blue

Note that capillary crossflow during CO_2 injection can occur at injection pressures lower than near-miscible pressures as long as there is a driving force (i.e. IFT gradient in oil phase). However, due to the weaker extraction of oil components at lower pressures, the driving force will be smaller, and therefore, the capillary crossflow would be weaker. The same mechanism could also occur during multiple-contact miscible injection cases. In these cases, as CO_2 contacts the oil, it extracts its lighter fractions and dissolves in the oil which at some point creates a miscible zone ahead of CO_2 front. The heavier oil lags behind, and there is a two-phase flow at the rear of the miscible zone. In this two-phase flow region, there is the extraction of extractable oil components into the CO_2 stream and therefore an IFT gradient across the undisplaced oil phase which leads to CO_2 capillary crossflow.

During CO_2 flow, due to the swelling of the oil layer in the narrowest regions of the porous medium, CO_2 snap off occurred which led to the trapping of CO_2 (Fig. 14). CO_2 residual trapping occurs during CO_2 underground injection which leads to the safe storage of CO_2 in the porous medium. Note that CO_2 bubbles can coalesce when they get close to each other and we observed this phenomenon.

Since CO_2 was injected into the waterflooded microfluidic chip, some trapped oil ganglia were shielded by water layers and were inaccessible to the CO_2 stream (Fig. 15). For CO_2 to meet these isolated oil ganglia, it must first diffuse into the oil layer surrounding the CO_2 stream; then, from the oil layer, it must diffuse into the water layer surrounding the oil ganglia, and finally, from the water layer, the CO_2 must diffuse into the oil. As CO_2 component reaches the oil, if the oil swelling is sufficient to rupture the water layer and bring the oil in contact with the main CO_2 stream, the oil ganglia are then produced. Therefore, the recovery of water-shielded oil ganglia is controlled by diffusion rates of CO_2 between different phases and the extent of oil swelling. As a result, the recovery rate of water-shielded oil ganglia is slow. These findings are consistent with the Campbell and Orr observations (Campbell and Orr 1985).

During near-miscible CO_2 injection, a strong extraction of light-to-intermediate (extractable) oil components into the CO_2 stream was detected which caused the CO_2 to become

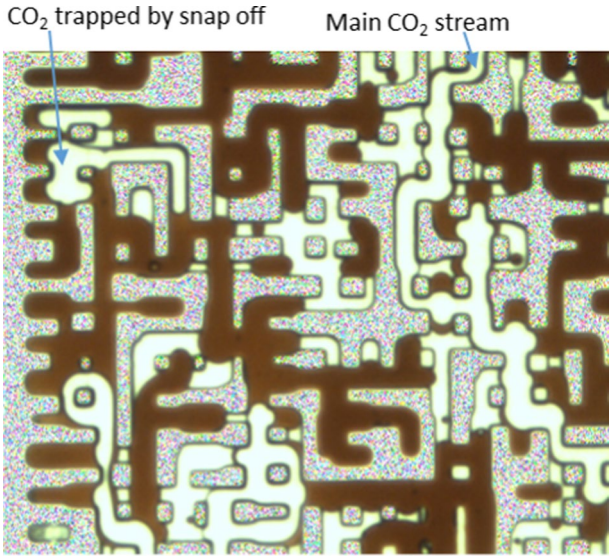

Fig. 14 CO_2 snap off that leads to CO_2 residual trapping

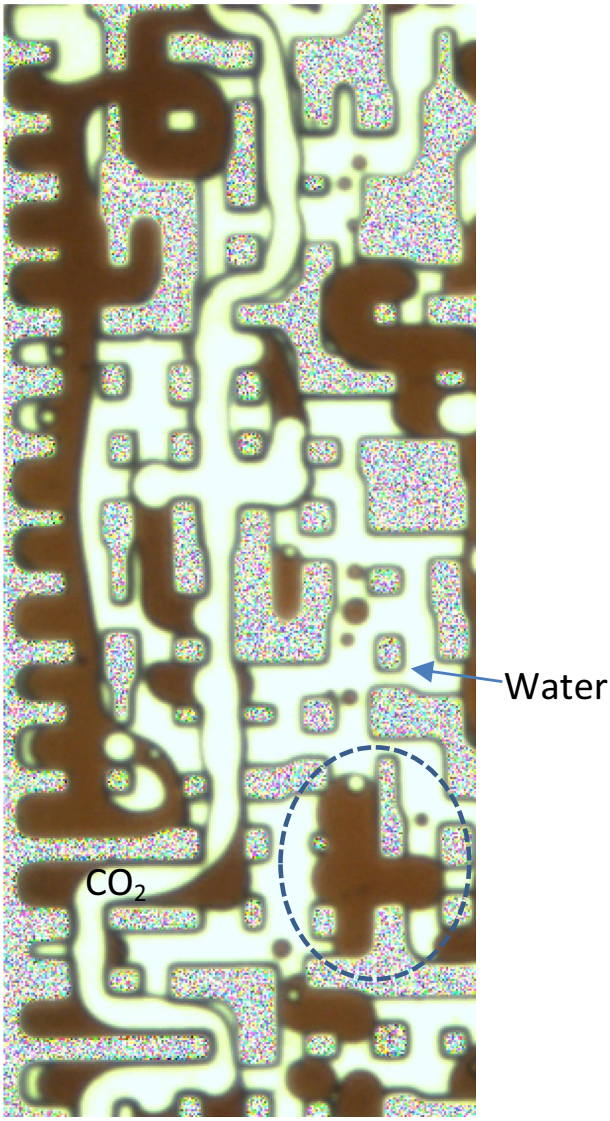

Fig. 15 Water-shielded oil ganglion (dashed region) during CO_2 injection

enriched in hydrocarbon components and oil becomes heavier (as seen by the change in the colour of the oil shown in Fig. 12). As more CO_2 came in contact with the interacting oil, this extraction continued and its effects on oil quality became more visible. Figure 16 is taken after several pore volumes of CO_2 came in contact with the oil. Since the light condition and camera settings were constant during the whole experiments, the only reason for the change in oil colour is the transfer of its extractable hydrocarbon components into the CO_2 stream. The same extraction behaviour was reported in micromodel work conducted by Bahralolom and Orr (1986). The observed extraction in this work was not significant enough to lead to miscibility. Interestingly, this extraction did not cause any detectable asphaltene precipitation or wettability change as opposed to the asphaltene precipitation reported by Robin et al. (2012). This reveals that these effects are a function of oil type and

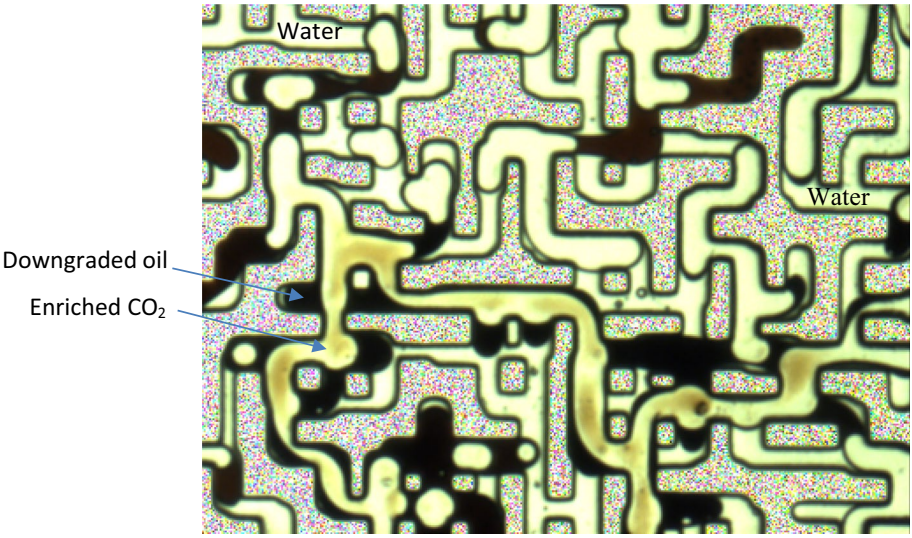

Fig. 16 CO_2–crude oil interactions during near-miscible CO_2 injection. Oil losses its light to medium hydrocarbon components to CO_2

composition. Note that at some places, a yellowish colour in the CO_2 stream was observed (refer to Figs. 13 and 16). This could be due to the films of heavy oil components left as a residue on the pore walls.

5 Conclusions

The outcomes of this study provide further insights on multiphase flow during near-miscible CO_2 EOR/storage showing that near-miscible CO_2 injection is potentially viable. Although miscibility does not occur during this scenario and pore-scale heterogeneity and adverse viscosity ratio lead to poor sweep efficiency for CO_2 at early times of injection, the diffusion of CO_2 into the oil phase and the extraction of light to medium oil components into the CO_2 phase create an interfacial tension gradient across the undisplaced oil phase. This interfacial tension gradient acts as the driving force for CO_2 capillary crossflow into the undisplaced oil and consequent production of the oil through the spreading oil layer. The same mechanism helps the production of the oil trapped in dead-end pores. As such, after CO_2 breakthrough, a significant amount of bypassed oil is produced via this mechanism. Capillary crossflow could also occur during immiscible and multiple-contact miscible scenarios as long as there is a driving force. It is expected that the driving force (i.e. interfacial tension gradient) and therefore additional oil recovery by capillary crossflow will be stronger at near-miscible conditions than immiscible.

At near-miscible conditions, the spreading coefficient value and wettability will determine the fluids' configuration in each pore for any sequence of the CO_2 invasion. As such, these factors will determine the CO_2–oil surface contact area and therefore will directly impact the oil recovery. In a water-wet porous medium when the spreading coefficient has a positive value, oil forms a layer between water occupying the corners and cervices and the gas phase flowing at the centre of the pore. Under this condition, the CO_2 flows inside

the oil, and a layer of oil spreads on the CO_2 stream which avoids CO_2 phase contacts the brine. As CO_2 flows and invades each pore, oil will be pushed ahead of the CO_2 front which leads to redistribution and reconnection of trapped oil ganglia and the formation of an oil bank ahead of CO_2 front. Under this three-phase flow condition, CO_2 displaces the brine through a multiple displacement mechanism and displaces the oil via a mix of bulk flow and layer flow.

References

Ahmed, T.: Fundamentals of reservoir fluid flow. In: Work Guid to Reserv Rock Prop Fluid Flow, pp. 117–246 (2013). https://doi.org/10.1016/b978-1-85617-825-9.00003-x

Akai, T., Xue, Z., Yamashita, Y., Yoshizawa, M.: Application of CO2 micro bubble for the innovative CO2-EOR. In: Abu Dhabi International Petroleum Exhibition and Conference, vol. 8 (2015). https://doi.org/10.2118/177672-ms

Al-Menhali, A.S., Krevor, S.: Capillary trapping of CO2 in oil reservoirs: observations in a mixed-wet carbonate rock. Environ. Sci. Technol. **50**(5), 2727–2734 (2016). https://doi.org/10.1021/acs.est.5b05925

AlQuaimi, B.I., Rossen, W.R.: Study of foam generation and propagation in fully characterized physical-model fracture. J. Pet. Sci. Eng. **2019**(175), 1169–1181 (2018). https://doi.org/10.1016/j.petrol.2018.06.025

Bachu, S.: Screening and ranking of sedimentary basins for sequestration of CO2 in geological media in response to climate change. Environ. Geol. **44**(3), 277–289 (2003). https://doi.org/10.1007/s00254-003-0762-9

Bahralolom, I.M., Orr, F.M.: Solubility and extraction in multiple-contact miscible displacements: comparison of N//2 and Co//2 flow visualization experiments. Soc. Pet. Eng. AIME SPE **1**(February), 363–370 (1986). https://doi.org/10.2118/15079-pa

Campbell, B.T., Orr, F.M.: Flow visualization for Co2/crude oil displacements. Soc. Pet. Eng. J. **25**(5), 665–678 (1985). https://doi.org/10.2118/11958-PA

Ceyssens, F., Puers, R.: Deep etching of glass wafers using sputtered molybdenum masks. J. Micromech. Microeng. (2009). https://doi.org/10.1088/0960-1317/19/6/067001

Ghasemi, M., Astutik, W., Alavian, S.A., et al.: Impact of pressure on tertiary-CO2 flooding in a fractured chalk reservoir. J. Pet. Sci. Eng. **167**(April), 406–417 (2018). https://doi.org/10.1016/j.petrol.2018.04.022

Golkari, A., Riazi, M.: Experimental investigation of miscibility conditions of dead and live asphaltenic crude oil–CO2 systems. J. Pet. Explor. Prod. Technol. **7**(2), 597–609 (2017). https://doi.org/10.1007/s13202-016-0280-4

Grigg, R.B., Gregory, M.D., Purkaple, J.D.: The effect of pressure on improved oilflood recovery from tertiary gas injection. SPE Reserv. Eng. **12**(03), 179–188 (1997). https://doi.org/10.2118/35426-PA

Hamdi, Z., Awang, M.: Oil recovery study by low temperature carbon dioxide injection in high-pressure high-temperature micromodels. Int. J. Energy Environ. Eng. **11**(11), 1123–1129 (2017)

Hemmati-Sarapardeh, A., Ayatollahi, S., Ghazanfari, M.H., Masihi, M.: Experimental determination of interfacial tension and miscibility of the CO2-crude oil system; temperature, pressure, and composition effects. J. Chem. Eng. Data **59**(1), 61–69 (2014). https://doi.org/10.1021/je400811h

Hill, B., Hovorka, S., Melzer, S.: Geologic carbon storage through enhanced oil recovery. Energy Procedia **37**, 6808–6830 (2013). https://doi.org/10.1016/j.egypro.2013.06.614

Huang, T., Zhou, X., Yang, H., Liao, G., Zeng, F.: CO2 flooding strategy to enhance heavy oil recovery. Petroleum **3**(1), 68–78 (2017). https://doi.org/10.1016/j.petlm.2016.11.005

Khather, M., Saeedi, A., Myers, M.B., Verrall, M.: An experimental study for carbonate reservoirs on the impact of CO2-EOR on petrophysics and oil recovery. Fuel **2019**(235), 1019–1038 (2018). https://doi.org/10.1016/j.fuel.2018.08.094

Kuuskraa, V.A., Godec, M.L., Dipietro, P.: CO2 Utilization from "Next Generation" CO2 enhanced oil recovery technology. Energy Procedia **37**, 6854–6866 (2013). https://doi.org/10.1016/j.egypro.2013.06.618

Li, X., Akbarabadi, M., Karpyn, Z.T., Piri, M., Bazilevskaya, E.: Experimental investigation of carbon dioxide trapping due to capillary retention in saline aquifers. Geofluids **15**(4), 563–576 (2015). https://doi.org/10.1111/gfl.12127

Ma, J., Wang, X., Gao, R., et al.: Study of cyclic CO2 injection for low-pressure light oil recovery under reservoir conditions. Fuel **174**, 296–306 (2016). https://doi.org/10.1016/j.fuel.2016.02.017

Metcalfe, R.: Effects of impurities on minimum miscibility pressures and minimum enrichment levels for CO2 and rich-gas displacements. Soc. Pet. Eng. J. **22**(02), 219–225 (1982). https://doi.org/10.2118/9230-pa

Metcalfe, R.S., Yarborough, L.: The effect of phase equilibria on the CO2 displacement mechanism. Soc. Pet. Eng. J. **19**(04), 242–252 (1979). https://doi.org/10.2118/7061-PA

Mojtaba, S., Behzad, R., Rasoul, N.M., Mohammad, R.: Experimental study of density-driven convection effects on CO2 dissolution rate in formation water for geological storage. J. Nat. Gas Sci. Eng. **21**, 600–607 (2014). https://doi.org/10.1016/j.jngse.2014.09.020

Nemati Lay, E., Taghikhani, V., Ghotbi, C.: Measurement and correlation of CO2 solubility in the systems of CO2 + toluene, CO2 + benzene, and CO2 + n-hexane at near-critical and supercritical conditions. J. Chem. Eng. Data **51**(6), 2197–2200 (2006). https://doi.org/10.1021/je0602972

Nobakht, M., Moghadam, S., Gu, Y.: Mutual interactions between crude oil and CO2 under different pressures. Fluid Phase Equilib. **265**(1–2), 94–103 (2008). https://doi.org/10.1016/j.fluid.2007.12.009

Perrin, J.C., Benson, S.: An experimental study on the influence of sub-core scale heterogeneities on CO2 distribution in reservoir rocks. Transp. Porous Media **82**(1), 93–109 (2010). https://doi.org/10.1007/s11242-009-9426-x

Rahman, T., Lebedev, M., Barifcani, A., Iglauer, S.: Residual trapping of supercritical CO2 in oil-wet sandstone. J. Colloid Interface Sci. **469**, 63–68 (2016). https://doi.org/10.1016/j.jcis.2016.02.020

Robin, M., Behot, J., Sygouni, V.: CO2 injection in porous media: observations un glass micromodels under reservoir conditions. SPE Improv. Oil Recovery Symp. **2**, 1–15 (2012). https://doi.org/10.2118/154165-ms

Sandrea, I., Sandrea, R.: Global oil reserves-1: recovery factors leave vast target for EOR technologies. Oil Gas J. **105**, 44–48 (2007)

Seyyedi, M., Sohrabi, M.: Pore-scale investigation of crude oil/CO2 compositional effects on oil recovery by carbonated water injection. Ind. Eng. Chem. Res. **56**(6), 1671–1681 (2017). https://doi.org/10.1021/acs.iecr.6b04743

Seyyedi, M., Mahzari, P., Sohrabi, M.: An integrated study of the dominant mechanism leading to improved oil recovery by carbonated water injection. J. Ind. Eng. Chem. **45**, 22–32 (2017a). https://doi.org/10.1016/j.jiec.2016.08.027

Seyyedi, M., Mahzari, P., Sohrabi, M.: A comparative study of oil compositional variations during CO2 and carbonated water injection scenarios for EOR. J. Pet. Sci. Eng. **2018**(164), 685–695 (2017b). https://doi.org/10.1016/j.petrol.2018.01.029

Seyyedi, M., Mahzari, P., Sohrabi, M.: A fundamental micro scale study of the roles of associated gas content and different classes of hydrocarbons on the dominant oil recovery mechanism by CWI. Sci. Rep. **9**(1), 5996 (2019). https://doi.org/10.1038/s41598-019-42226-6

Seyyedi, M., Mahmud, H.K.B., Verrall, M., et al.: Pore structure changes occur during CO2 injection into carbonate reservoirs. Sci Rep. **10**(1), 1–14 (2020a). https://doi.org/10.1038/s41598-020-60247-4

Seyyedi, M., Giwelli, A., White, C., Esteban, L., Verrall, M., Clennell, B.: Effects of geochemical reactions on multi-phase flow in porous media during CO2 injection. Fuel (2020b). https://doi.org/10.1016/j.fuel.2020.117421

Seyyedsar, S.M., Sohrabi, M.: Intermittent CO2 and viscosity-reducing gas (VRG) injection for enhanced heavy oil recovery. Fuel Process. Technol. **164**, 1–12 (2017). https://doi.org/10.1016/j.fuproc.2017.04.013

Shyeh-Yung, J.-G.J.: Mechanisms of miscible oil recovery: effects of pressure on miscible and near-miscible displacements of oil by carbon dioxide. In: SPE's Annual Technical Conference and Exhibition, vol. 15 (1991). https://doi.org/10.2118/22651-ms

Sohrabi, M., Danesh, A., Tehrani, D.H., Jamiolahmady, M.: Microscopic mechanisms of oil recovery by near-miscible gas injection. Transp. Porous Media **72**(3), 351–367 (2008). https://doi.org/10.1007/s11242-007-9154-z

Sohrabi, M., Riazi, M., Jamiolahmady, M.: Mechanisms of oil recovery by carbonated water injection. In: SCA Annual Meeting, pp. 1–12 (2009). http://www.scaweb.org/assets/papers/2009_papers/SCA2009-26.pdf. Accessed 27–30 Sept 2009

Song, W., Kovscek, A.R.: Functionalization of micromodels with kaolinite for investigation of low salinity oil-recovery processes. Lab Chip **15**(16), 3314–3325 (2015). https://doi.org/10.1039/c5lc00544b

Tenasaka, I.: Global CCS Institute Bridging the Commercial Gap for Carbon Capture and Storage July 2011 (2011)

Tovar, F.D., Eide, O., Graue, A., Schechter, D.S.: Experimental investigation of enhanced recovery in unconventional liquid reservoirs using CO2: a look ahead to the future of unconventional EOR. In: SPE Unconventional Resources Conference (2014). https://doi.org/10.2118/169022-ms

Welch, S.A., Sheets, J.M., Place, M.C., et al.: Assessing geochemical reactions during CO2 injection into an oil-bearing reef in the Northern Michigan basin. Appl. Geochem. **2019**(100), 380–392 (2018). https://doi.org/10.1016/j.apgeochem.2018.12.008

Yongmao, H., Zenggui, W., Binshan, J., Yueming, C., Xiangjie, L.: Laboratory Investigation of CO2 flooding. In: Nigeria Annual International Conference and Exhibition, vol. 6 (2004). https://doi.org/10.2118/88883-ms

Zhang, P.Y., Huang, S., Sayegh, S., Zhou, X.L.: Effect of CO2 impurities on gas-injection EOR processes. in: SPE/DOE Symp Improv Oil Recover (2004). https://doi.org/10.2118/89477-ms

Zhang, Y., Gao, M., You, Q., et al.: Smart mobility control agent for enhanced oil recovery during CO2 flooding in ultra-low permeability reservoirs. Fuel **2019**(241), 442–450 (2018). https://doi.org/10.1016/j.fuel.2018.12.069